
Article:
Liu, X., Conte, M., Weng, W. et al. (9 more authors) (2015) Molybdenum blue nano-rings: an effective catalyst for the partial oxidation of cyclohexane. Catalysis Science and Technology, 5 (1). pp. 217-227. ISSN 2044-4753

https://doi.org/10.1039/c4cy01213e

Catalysis Science and Technology RSCPublishing

ARTICLE

Molybdenum blue nano-rings: an effective catalyst for the partial oxidation of cyclohexane†

Cite this: DOI: 10.1039/x0xx00000x

Received 00th January 2012,
Accepted 00th January 2012

DOI: 10.1039/x0xx00000x

www.rsc.org/

Xi Liu,[a] Marco Conte,[a,b] Weihao Weng,[c] Qian He,[c] Robert L. Jenkins,[a] Masashi Watanabe,[c] David Morgan,[a] David W. Knight,[a] Damien Murphy,[a] Keith Whiston,[d] Christopher J. Kiely[b] and Graham J. Hutchings[a]*

Molybdenum blue (MB), a multivalent molybdenum oxide with a nano-ring morphology is well-known in analytical chemistry but, to date it has been largely ignored in other applications. In the present work, MB has been characterized by STEM-HAADF imaging for the first time, showing the nano-ring morphology of this complex molybdenum oxide and the ordered super-molecular framework crystals that can result from the self-assembly of these MB nano-ring units. The potential of MB as an oxidation catalyst has also been investigated, where it is shown to have excellent catalytic activity and stability in the selective oxidation of cyclohexane to cyclohexanol and cyclohexanone which are important intermediates in the production of nylon.

Catalysis Science and Technology RSCPublishing

ARTICLE

1. Introduction

In the present paper, we demonstrate that a material that has been known for centuries, but which until now has been largely ignored for catalyst applications, possesses exciting catalytic properties. The material in question is molybdenum blue (MB)[1] which is well-known in colorimetric and quantification assays, particularly for phosphorus.[2-3] It was first synthesized over 200 years ago,[4] however, its structure has been enigmatic, with the first convincing models of its atomic arrangement emerging in 1995.[5] The classic X-ray diffraction studies of MB by Müller et al. unveiled the linkage of $[(Mo^{V}/Mo^{VI})_{m}O]_{n}$ units into giant wheel-shaped clusters by hydrogen bonding.[5] More recently, Zhong et al. have used scanning tunnelling microscopy (STM) to directly image individual isolated MB rings,[6] but to date there have been no direct observations of the MB nano-structure using transmission electron microscopy. MB is considered to be comprised of complex assemblies of wheel-shaped mixed-valence: Mo_{154} polyoxomolybdate, $[Mo^{VI}_{126}Mo^{V}_{28}O_{462}H_{14}(H_2O)_{70}]^{14-}$ anion clusters.[5,7,8] We reasoned that MB nano-ring structures and their complex assemblies should in principle be observable using high angle annular dark field (HAADF) imaging in the scanning transmission electron microscope (STEM). To date there has been limited progress in the characterization of the microstructure of these mixed-valency molybdenum compounds by electron microscopy. Nevertheless, high-resolution TEM images acquired in these previous studies show poor correlation with the STM images obtained by Zhong et al.,[6] as no discrete nano-ring structures were observed. While there has been considerable interest in the structure of MB nano-rings and their molecular assemblies, its use as a catalyst has not been considered in any great detail. In this paper, we present the first clear HAADF-STEM images of MB nano-ring structures. In addition, we demonstrate that the $[(Mo^{V}/Mo^{VI})_{m}O]_{n}$ units present within the nano-ring structure can be highly active for the catalysis of hydrocarbon oxidation.

Selective oxidation is an important process for the functionalization of chemical feedstocks and there is a continual need to identify new catalysts particularly if they demonstrate interesting selectivity to desirable partial oxidation products. Catalysts have been formulated based on mixed oxides and supported metals for a wide range of such reactions.[9] There has been particular interest in utilising molybdenum oxide containing catalysts, including the use of heteropolyacids.[10,11,12] In the majority of these reports the molybdenum is usually present as Mo^{VI} species. However, it has been demonstrated that an activating pre-treatment step in an H_2 or a hydrocarbon atmosphere is very important in establishing the activity and selectivity of oxidized molybdenum carbides.[9] It was noted that this type of activation pre-treatment generates some Mo^{V} species as well as Mo^{VI} which results in materials with strong blue colorations due to electron exchanges between nearby Mo^{V} and Mo^{VI} cations in the structure.[9,13] We also note that in many previous studies of other molybdenum-based materials, including molybdenum sulfides and molybdenum oxides, there have been reports of a strong blue colouration, thereby suggesting the possible formation of MB-like species during their preparation.[9-12] Consequently, we reasoned that MB, which exhibits significant electron hopping between Mo^{V} and Mo^{VI} sites via Mo^{V}-O-Mo^{VI} bridging bonds, might represent a material that could be highly active for selective redox chemistry.[6] In particular, we considered that MB should be active for the oxy-functionalization of alkanes to selective oxidation products such as alcohols, ketones and acids, and additionally that this process should be feasible under mild reaction conditions. Identification of new catalysts for this type of chemistry is of considerable interest to both academia and industry.[9, 14-20] A key reaction in this class is the selective oxidation of cyclohexane, as this is of great importance as an intermediate step in nylon manufacture which has an annual production of over 3M tonnes and is therefore a reaction of immense practical and commercial significance.[18] The current industrial process for cyclohexane oxidation uses radical autoxidation promoted by cobalt ions which significantly impedes selectivity control.[14, 15, 18-21] In this paper, we show that MB can provide a novel catalytic oxygenation of cyclohexane giving high selectivity to partial oxidation products and we discuss this catalysis in relation to the unique structure of this fascinating material.

2. Experimental Methods

2.1 Synthesis of molybdenum blue

Molybdenum blue (MB) was prepared via a facile synthesis method. Powdered metallic molybdenum (Sigma, assay 99.99%) was mixed with diluted hydrogen peroxide (Aldrich 30 wt%, trace metals < 10 ppm) and afterwards the suspension was stirred overnight at room temperature. After filtration, the blue solution formed was evaporated to dryness using a rotary evaporator at room temperature in order to obtain a fine blue powder. Compared to other preparation protocols for MB,[5] the main advantage of the method employed in this work, is that the MB prepared is relatively free from impurities.

2.2 Characterization of the catalyst

2.2.1 Scanning transmission electron microscopy

High angle annular dark field (HAADF) and bright field (BF) imaging experiments were carried out in an aberration corrected JEOL JEM-2200FS scanning transmission electron microscope (STEM). This instrument is equipped with a field emission gun (FEG) and was operated at a 200 kV accelerating voltage. Samples for STEM characterization were prepared by putting a drop of an aqueous solution of MB onto a holey carbon TEM grid and allowing the water to evaporate. Additional 'gentle' STEM experiments at 80kV were carried out in an aberration corrected JEOL JEM-200F ARM.

2.2.2 Diffuse reflectance spectroscopy

UV-Vis diffuse reflectance spectra were collected using a Harrick Praying Mantis cell mounted on a Varian Cary 4000 spectrophotometer. The spectra were collected from 850 to 200 nm at a scan speed of 60 nm min^{-1}. Background correction was carried out using Teflon powder (Spectralon). The sample was mounted on a 3 mm diameter diffuse reflectance sampling cup.

2.2.3 X-ray powder diffraction

X-ray powder diffraction (XRPD) patterns of MB were collected using an X'Pert Panalytical diffractometer operating at 40 kV and 40 mA with CuK_α radiation, with the sample fixed to a Macor sample holder mounted in a XRK900 Anton Paar in-situ XRD cell.

2.2.4 X-ray photoelectron spectroscopy

X-ray photoelectron spectroscopy (XPS) was performed with a Kratos Axis Ultra DLD spectrometer using a monochromatised AlK_α X-ray source (120 W) with an analyser pass energy of 160 eV for survey scans and 40 eV for detailed elemental scans. Binding energies are referenced to the C(1s) binding energy of carbon, taken to be 284.7 eV.

2.3 Catalyst testing

Standard reaction conditions for the oxidation of cyclohexane were as follows. Cyclohexane (Alfa Aesar, 8.5 g, HPLC grade) was reacted in a glass bench reactor with catalysts (6 mg). To control accurately the amount of the MB catalyst we used, a dilute aqueous solution of MB with a known concentration of MB was prepared. The desired volume of the MB solution was dispensed as a drop into the glass reactor which was then evaporated to dryness at 30 °C. It should be noted that while MB is soluble in water, it is insoluble in cyclohexane and so using our reaction conditions we consider that the molybdenum blue is present as a heterogeneous catalyst. The reaction mixture was magnetically stirred at 140°C and 3 bar O_2 for 17 h. The reaction mixture was analysed by gas chromatography (Varian 3200) with a CP-Wax 42 column. It should also be noted that acid products, such as adipic acid, were converted to their corresponding ester for quantification purposes.[22] For a comparison with the industrial process, the oxidation reactions were also performed by using promoters (6 mg) comprising cobalt naphthenate and ferric acetylacetonate, at 140°C and 3 bar O_2 for 17 h.

Re-usability testing was also performed in an identical glass reactor. Cyclohexane (8.5 g) and MB (60 mg) were reacted at 140 °C and 3 bar O_2 for 17 h. After reaction, the 'used' catalyst was washed with cyclohexane and dried. The catalytic activity of the used MB was re-tested under the standard reaction conditions) and the products were analysed by gas chromatography. Subsequent re-usability tests were carried out on the same material using another iteration of the procedure.

2.4 Characterization of the reaction products by GC/MS and NMR

In the present work, we conducted a very careful analytical procedure, in order to ensure that we collected all the possible products and give both a reliable analysis and a complete carbon mass balance.

Liquid sample analysis: after reaction, the liquid and solid products were carefully isolated. A known concentration of chlorobenzene (internal standard) was added to the liquid sample prior to analysis by GC-FID (Varian 3200 with a CP-Wax 42 column). Cyclohexane conversion and selectivities to the products, e.g. cyclohexanol and cyclohexanone, were calculated on the GC response relative to that generated by the chlorobenzene internal standard.

Solid sample analysis: After removal of the liquid sample, the reactor interior and solid deposit (solid products and catalyst mixture) were carefully washed with cyclohexane to remove any products that are soluble in cyclohexane. As described in the literature, polar products, including formic acid, glutaric acid, succinic acid, hydroxyl caproic acid and adipic acid, would remain in the solid.[22] Afterwards, the reactor was washed several times with methanol (15 mL batches) to collect all the polar products in the methanol solutions. In the present work, very small amounts of catalyst material (6 mg) were used, implying that the amount of product that remains absorbed on the catalysts will be negligible. Those acid products present in the methanol solution cannot be directly analysed by GC due to strong absorbance and high boiling point. To overcome this problem, derivatization of OH-containing compounds into trimethylsilyl or alkyl esters prior to analysis is necessary, making the acidic by-products less polar, more volatile, and hence more thermally stable - therefore enabling quantification by GC.[22, 23] In the present work, all the acid products were converted into their corresponding methyl derivatives with an excess BF_3 in methanol (14%) prior to GC-FID analysis.[22] Adipic acid concentration and thus selectivity were determined relative to the chlorobenzene internal standard concentration. After analysis, we found almost all the solid product is adipic acid (Figure. S2). No glutaric acid, succinic acid, hydroxyl caproic acid was identified. Additionally, we also derivatized the liquid sample to account for trace amounts of acids dissolved in cyclohexane. The selectivities to adipic acid presented in our various tables of results cover the presence of adipic acid in both solid and liquid samples.

Gas sample analysis: In the literature, significant production of gaseous products has been observed.[22] Thus, an analysis of gaseous products generated was deemed to be essential. After reaction, the headspace above the reaction mixture was analysed for CO/CO_2 using a GC-FID equipped with a methaniser. However, we did not identify any CO/ CO_2 or CH_x products in our experiments.

Finally, GC/MS analysis was employed to identify any minor reaction by-products and their detailed quantification is listed in Tables S1 and S2. GC/MS analysis was carried out on a Waters GCT premier system using an Agilent DB-5MS capillary column [30m (L) x 0.25mm (OD) x 0.25 μm (film)]. The oven temperature profile employed to achieve the required separation was 40°C held for 5 min followed by a temperature ramp of 8°C min^{-1} ramp up to 280°C, with this final temperature being held for 5 min. The injector temperature employed was 200°C. Because the total conversion is calculated from the molar amount of cyclohexane which decreases during the reaction, the total selectivity is equal to the mass balance of all the observed products which means that our quoted conversion values may possibly be very slightly over-estimated.

Product screening was also performed using a Bruker Avance III 600 MHz NMR spectrometer equipped with a QCI cryo-probe. The extracted solid product in the MB-catalysed cyclohexane oxidation was also analysed by NMR. Both ^{1}H-NMR spectra are presented in Figure S1 and these show that we

have not missed any higher molecular weight products that are not amenable to GC analysis. In the case of (i) MB catalysed cyclohexane oxidation and (ii) cobalt naphthenate catalysed cyclohexane oxidation, no additional products were detected.

3. Results and discussion

3.1 Characterization of the structure of MB using scanning transmission electron microscopy

We have applied STEM-HAADF imaging for the first time to examine the nanostructure of MB samples. The first convincing structural models of MB, published by Müller et al. in 1995, were primarily based on powder X-ray diffraction and the evidence suggested that the material was comprised of complex assemblies of wheel-shaped mixed-valence polyoxomolybdate $[Mo^{VI}_{126}Mo^{V}_{28}O_{462}H_{14}(H_2O)70]^{14-}$ anion clusters.[5,6] In our work, samples for STEM characterization were prepared by putting a drop of a very dilute aqueous solution of MB onto a continuous carbon TEM grid and allowing the water to evaporate. Using this methodology any pre-existing self-assembled superstructures of rings are not retained at this high level of dilution and this method aids the study of the individual nano-rings rather than the superstructures. The MB ring structures are essentially invisible against the carbon support by conventional bright field phase contrast imaging (Figure.1a), but are clearly visible in the HAADF image (Figure 1b) by virtue of the strong atomic mass (z-) contrast generated by the Mo atoms in relation the other elements in the ring molecule and the C atoms in the underlying support film.

In very dilute samples the individual Mo_{154} wheel shaped clusters became well dispersed and can be imaged as separate entities (Figure 2a), whereas in specimens generated from more concentrated MB solutions, the rings overlap giving a more confused picture due to their agglomeration into new superstructures as the solvent evaporates during the drop casting process (Figures 2b-d).[6] Low pass filtered HAADF images of individual MB units were obtained in which the ring structure can now be clearly observed (Fig. 3a). The rings are observed to have external and internal diameters of ~3.6 nm and ~2.0 nm respectively which matches well with the expected dimensions of the Mo_{154} model structure (inset of Figure 3a). It should be noted that these ring structures are highly sensitive to prolonged electron irradiation damage at 200kV and within a minute of exposure to the electron beam will collapse and transform into dense crystallites of MoO_3 or even MoO_2 as shown in Figure sequence 3(a)-(e).[24] This observation is in good agreement with previous HRTEM studies of reduced molybdenum oxides and molybdenum-blue-like species which have noted the propensity of these materials to exhibit electron beam modification.[8] Aberration corrected STEM-HAADF imaging at 80kV has also been performed on our MB materials (Figure 4), and although the lower accelerating voltage was found to reduce the rate of electron beam damage somewhat, it did not eliminate the damage effects completely. We have also performed comparisons of the MB structure before and after the materials have been used as a catalyst for the oxidation of cyclohexane (Figure 5:- the catalysis experiments are described in section 3.2). It was not possible to discern any significant difference between the pre- and post- use structures, confirming that the Mo_{154} ring morphologies are robust and remain intact under the mild reaction conditions employed (section 3.2).

When more concentrated solutions of MB were drop-cast onto the carbon support films, we found evidence that the $[Mo^{VI}_{126}Mo^{V}_{28}O_{462}H_{14}(H_2O)70]^{14-}$ anion clusters were prone to re-assemble under the influence of hydrogen bonding into periodic layered super-structures typically containing 20 nm-scale mesopores (see Figures 5 and 6).[5] The ring spacings and separation in Fig. 6(a) are broadly consistent with the structure (Figure 6(b)) of the $Na_{16}[Mo^{VI}_{124}Mo^{V}_{2}8O_{429}(3\text{-}O)_{28}H_{14}(H_2O)_{66.5}]c.a.300H_2O$ ($\{Mo_{152}\}$) compound as determined previously by XRD, although the counter-ion present in our case is more likely to be H^+.[5, 7 25] It should be noted that such self-assembled superstructures could not be directly imaged in a previous STM study of Zhong et al., where the individual Mo_{154} moieties had to be well separated on flat surface in order to acquire an image.[6, 9] The mixed Mo^{VI}/Mo^{V} valence state, coupled with a high effective surface area (240 $m^2\ g^{-1}$) should in principle should make this a highly attractive and effective catalyst morphology for the oxidation of cyclohexane.

3.2 Cyclohexane oxidation using MB as a catalyst

We noted that there are abundant electron transitions between neighbouring Mo^{VI}/Mo^{V} cations in MB and that it has a redox potential that is very similar to Fe^{III}/Fe^{II} in Keggin Polyoxoanions.[26, 27] This suggests that MB could be a good candidate as a catalyst in some challenging selective oxidation reactions. For this reason we have explored whether or not the Mo^{V}-O-Mo^{VI} bridging structure in MB is active for selective redox chemistry[6, 8-13] by testing it for the oxy-functionalization of cyclohexane.

In this work the activity of MB as a catalyst for cyclohexane (C_6H_{12}) oxidation has been contrasted with that of cobalt naphthenate which is currently used as a homogeneous catalyst in commercial processes. We also compare the activity of MB with that of $Fe(acac)_3$, which is widely used as an iron resource for the aerobic oxidation of cyclohexane.[14] For the experiments with MB, as we were investigating the use of very low amounts of the material as a catalyst, we first made a significantly dilute aqueous solution of MB and put a small drop of this with desired volume into the glass reaction vessel to give the required amount of MB. The solution was then evaporated and hence this pre-treatment is analogous to that used in the preparation of the STEM samples and we know that for dilute MB samples that this results in the formation of discrete nano-ring structures. Hence this permits us to study the catalytic performance of the individual nano-ring structures without the complication of the presence of the more complex self-assembled super-structures. In our initial experiments with MB we observed a marked catalytic activity of 6% conversion with 93% selectivity to oxygenated products for this reaction (Table

1, and ESI† Table S1, Figs S1(a)-(b) and Fig. S2). At this level of cyclohexane conversion the performance is similar to that of the cobalt naphthenate commercial catalyst and ferric acetylacetonate (Table 1 and ESI† Table S2, Figs S1(c)-(d)). We analysed the reaction mixtures in detail using a range of analytical techniques to ensure that all products were correctly identified (see section 2). The major products detected were cyclohexanol, cyclohexanone and adipic acid. Traces amounts of hexyl esters were also detected. Furthermore, we have ensured that the mass balance was closed and that any differences observed in selectivity between MB and cobalt naphthenate were reproducible and statistically significant.

These catalytic data show that MB can be a promising material for the oxidation of this organic substrate, but it was also important to determine if catalysts used in batch reaction conditions can be effectively re-used. From the results shown in Table 2, it is apparent that the MB catalyst is fully re-usable based upon the measurements taken over four sequential usage cycles.Moreover, HAADF images of the MB before and after use in the oxidation of cyclohexane (Figures 5a and 5b respectively) show that the characteristic Mo_{154} ring structure has been retained even after the material has been used as a catalyst. The oxidation state of the metal also did not change during the reaction. In fact, XPS experiments (Figure 8) show that no remarkable differences were observed between the XPS profiles of the fresh and used MB material, with the ratio of Mo^{V} : Mo^{VI} cations remaining at about 1:4, which is consistent with the previously reported molar ratio of 1:4 as confirmed by the cerimetric titration method.[28]

3.2.1 Catalytic tests in presence of $CBrCl_3$

To appreciate the full significance ofthe MB catalytic data, it should be noted that cyclohexane oxidation by Co-naphthenate and $Fe(acac)_3$ operates via an autoxidation pathway promoted by the metal centre. As a consequence, for these catalyst materials, no selectivity control is allowed, and in turn it is difficult to control the final product distribution. Therefore, considering the similarities in the catalytic activity between these metal promoters and MB, we were prompted to investigate whether or not MB also carries out cyclohexane oxidation by means of a pure autoxidation pathway, as MB contains the Mo^{V}-O-Mo^{VI} motif, which is absent in the case of Co-naphthenate and $Fe(acac)_3$ which only have isolated mono-oxidation centres. In order to gather information on this important aspect, test were carried out (Table 3) in the presence of $CBrCl_3$, as radical scavenger which can quench carbon centred radicals by means of bromo-hydrocarbon formation.[29, 30] It should be noted that the use of dialkyl nitroxides for the capture of carbon centered radicals was deliberately avoided for this particular reaction. This is because the reaction conditions (i.e. solvent-free at a reaction temperature of ca. 140^{o}C), and the presence of metal centres can trigger hydrogen abstraction reactions[31] as well as the oxidation of the alcohol to the ketone,[32] and we wanted to minimize the possibility of of undesirable parallel reaction pathways existing in these radical quenching experiments.

In the presence of $CBrCl_3$, we observed that the activity of MB remains basically unaltered by the addition of the scavenger, whereas the activity of Co-naphthenate and $Fe(acac)_3$ is severely suppressed, with their conversions reduced by about one order of magnitude (Table 3). Even more significant, in presence of the scavenger the selectivity for Co-naphthenate and $Fe(acac)_3$ is now shifted towards cyclohexanone as the major product (ca. 10%), whereas, in case of MB the selectivity is shifted even more towards the more desirable cyclohexanol (i.e from 52% to 58%), which would suggest a real catalytic control exists in the MB system.

3.2.2 Control tests for solubilized Mo species

In view of these data, control tests combining a hot filtration step with a lower reaction temperature were carried out. The aim here was two-fold: (i) to further discriminate between a catalytic route induced by MB, and a pure autoxidation pathway; and (ii) to rule out any activity by oligomer molybdenum species if present. In this experiment, the catalytic oxidation of cyclohexane was performed at a lower reaction temperature (i.e. 120°C instead of 140°C) in order to suppress the autoxidation component. As expected the yield of products was significantly lower (ca. 0.4 %), although it was observed that cyclohexanol was the sole product over a 30 h reaction time at the lower temperature (Figure 9). This result confirms that catalytic oxidation is occurring in the presence of MB, since with an autoxidation pathway both the alcohol and ketone would be observed. For comparison, a blank experiment was also conducted using the same reaction conditions, which showed negligible activity even after 24 h of reaction (Figure 9c). After this time both cyclohexanol and cyclohexanone were formed, which is in good agreement with the occurrence of autoxidation. Hot filtration was performed after 12 h reaction of the initial reaction in order to remove the MB catalyst from the reaction mixture. Following this, the reaction was continued under the same reaction conditions. After a further 12 h reaction in the absence of MB (Figure 9b), no significant change in catalytic activity was observed, and the conversion remained unmodified at ca. 0.08%. The hot filtration experiment therefore provides further evidence that the presence of MB plays a key role in the catalytic oxidation of cyclohexane. As no further reaction was observed in the absence of the MB catalyst, it is clear that MB is required to observe conversion, and hence the reaction that is observed is not due to an underlying homogeneously catalysed pathway from any solubilised Mo species. On the other hand the apparent similarities between oxidation tests in present or absence of MB (Figure 9d), i.e. an increase in activity after ca. 25 h reaction time, are to be ascribed to autoxidation processes which are invariably operating for these class of reaction. In fact, for our tests, in presence of MB the increase in conversion after 25 h reaction time is due to an increase of alcohol.

Whereas in absence of MB the increase in activity is due to an increase of cyclohexanone.

3.2.3. Tests on fresh and thermally treated MB

The inference from the body of experimental evidence presented so far (i.e. conversion in presence of scavenger, reusability, selectivity effect, and hot filtration) is that MB operates the oxidation of cyclohexane via a different pathway if compared to $Fe(acac)_3$ and Co-naphthenate. In particular, Fe- and Co- based materials are promoters of the autoxidation route, whereas MB would appear to create a new reaction pathway by means of a real catalytic process enhancing alcohol formation. This could have important consequences for obtaining a catalyst capable of introducing a real selectivity control to such an important reaction.

In order to identify the underlying source of this behaviour, we have systematically studied the reactivity of MB nanorings, especially considering the specific structure of MB described in section 3.1. The first comparison was a control reaction using molybdate silicate blue ($SiMo_{12}O_{40}$) which is stable in our reaction environment and also exhibits a mixed valence Mo^V-O-Mo^{VI} structure.[33] The first observation is that this compound also shows similar conversion values of MB and also is not quenched by adding $CBrCl_3$ (see Tables 1 and 3). Moreover, the $SiMo_{12}O_{40}$ is also capable of creating a higher selectivity towards the alcohol, unlike Co-naphthenate and $Fe(acac)_3$, thus suggesting that the structural motif of mixed valence Mo^V-O-Mo^{VI} is important for the catalysis. Although it should be stressed that this effect for $SiMo_{12}O_{40}$ is fully evident in presence of radical scavenger only (table 3). In fact, it is under these conditions that it is possible to discriminate between autoxidation pathways and the activity induced by $SiMo_{12}O_{40}$.

On the other hand, the presence of oxygen in the MB lattice could also play a role in the process to explain this reactivity. In other words, if oxygen is removed from the lattice during the reaction, that in turn disrupts the Mo^V/Mo^{VI} moiety, which could alter the catalytic activity, possibly in terms of both conversion and selectivity. Therefore, to demonstrate that the oxygen from the MB structure is playing a role in the catalytic activity, we have carried out one further set of experiments. It is known that treating MoO_3 at temperatures above 140 ^oC under anaerobic conditions can deplete some of the lattice oxygen and thus affect its reactivity.[34]. These effects have been investigated for a temperature of 180 ^oC and this did not disrupt the three-dimensional lattice framework of the metal oxide.[35] Consequently, we thermally treated some MB at 180^{o}C for 48 h under a flow of He with the aim to achieve the same results observed for MoO_3, i.e. alteration of the Mo^V/Mo^{VI} moiety without collapse of the three dimensional MB framework.[36] The material was then examined by means of XRD and STEM in order to determine if the ring structures and molecular crystal framework superstructure were left intact after heating. In addition, it was further characterized by means of XPS and DR-UV to assess if the Mo^V/Mo^{VI} motif was disrupted or not, and tested again as a catalyst afterwards.

A comparison of the XRD patterns before and after thermal treatment shows that these two patterns are nearly identical (ESI†, Fig. S3 and Fig S4). This suggests that the overall MB structure (both the nanoring and super-structure) remained intact, and if any changes took place, this was related to O removal only, which can be accommodated without any large scale collapse of the structure. It should be stressed that the powder X-ray patterns that we collected for our MB samples (ESI† Fig. S3) are in full agreement with the XRD characterization carried out by Müller et al. on dry powders of MB,[6] i.e. diffuse scattering maxima at ca. 26^o, 29.5^o, 2θ and a broad set at 51^o 2θ degrees. In addition, by STEM we still see rings of similar dimension after the heat treatment in He (ESI† Fig S5(a)-(d)). However, with respect to the ratio of Mo^V/Mo^{VI} units present we do see a measurable difference. In the fresh sample, by XPS analysis (10) we observe that the Mo^V molar fraction is 20%, whereas after thermal treatment in He, it increases to 30%. Hence a clear increase in Mo^V and corresponding decrease in Mo^{VI} species is observed in the thermally-treated MB sample, the other XPS parameters, such as peak position and number of species present, remain unchanged, implying that the MB ring structure remains intact, and that the change in Mo^V/Mo^{VI} ratio is due to some removal of oxygen from the backbone of the ring lattice during the thermal treatment in He.

Additional evidence from DR-UV spectra (e1) provides a further important indication to what has happened to the MB material during this detrimental thermal treatment. The inter-valence charge transfer (IVCT) bands at 600-700 nm,[37] a characteristic finger-print region for molybdenum-blue compounds,[38] have merged into one band, confirming that a change in electronic properties has occurred. As these inter-valence bands are due to Mo^V-O-Mo^{VI} entities, their modification can be attributed to either loss of lattice oxygen, or breaking of some of the Mo^V-O-Mo^{VI} linkages.

All this data suggests that the thermal treatment in He left the ring structure intact, but disrupted the Mo^V-O-Mo^{VI} centres thus providing us with the opportunity to further assess the role of these Mo^V-O-Mo^{VI} moieties on the catalytic activity. Catalytic testing for the MB thermally treated in He showed that the conversion was basically unmodified (ca. 6%), whereas the selectivity to the alcohol was markedly decreased from 52% to 22%, (compare entries 1 and 6 in Table 1) and the selectivity is now shifted towards cyclohexanone and adipic acid (at ~ 49% and. 20% respectively) the latter of which was initially absent. This selectivity change is a key experimental observation, because if MB were functioning solely as an initiator, i.e. a promoter of autoxidation pathways like $Fe(acac)_3$ or Co-naphthenate, then the selectivities would remain the same, which is not observed. This experiment also serves to show that the number of Mo^V-O-Mo^{VI} moieties present is a key factor for determining the amount of alcohol formation. In fact, for Co-naphthenate or $Fe(acac)_3$ the reaction has been established to proceed by means of a Haber-Weiss cycle[39, 40] which involves homolytic cleavage of the cyclohexyl hydroperoxide intermediate. In contrast, for MB, the reaction

could conceivably take place via an oxo-metal species and thus proceed via a different mechanism to the autoxidation pathway.[18,22] On this particular aspect, we should note that in this work solvent-free conditions have been employed and as such we have not explored the kinetics of the reaction when using diluted cyclohexane. The use of a solvent has not been attempted in this study, as it is known that solvents can have a strong unintended effect on the final product distribution,[41,42] and we wanted to avoid further collateral complexity and undesired autoxidation reactions. However, we have studied the catalytic activity of MB as a function of reaction temperature (Figure 12a), and this shows a fascinating mono-hydroxylation of cyclohexane when using MB as a catalyst, which is clearly different from the autoxidation pathway which gives both alcohol and ketone as primary products.[21] Hence we consider that this also indicates that MB is a real catalyst in the partial oxidation of cyclohexane. The activation energy of this process in the presence of MB is determined to be ~95 kJ/mol (Figure 12b). Moreover, MB does not seem to be affected by oxygen diffusion limitations observed for some metal oxide based catalysts[43]under our reaction conditions. And this could further extend its applicability.

4.0 Conclusions

Our results show that MB, a material that has largely been neglected as a catalyst to date, is a selective catalyst for C-H bond oxo-functionalisation, which has direct relevance for a number of important industrial processes. In addition we have provided the first scanning transmission electron microscopy images of MB which show that the structure stays intact during use and that the catalysis we observe is associated with the structural motif of mixed valence Mo^{V}-O-Mo^{VI} entities which are present in MB nanorings and related structures. Furthermore, a remarkable difference between the catalytic behaviour of MB and commercial Co-naphthenate and $Fe(acac)_3$ catalysts was observed that allows some degree of prodict selectivity control when using MB. We consider that these observations will spur the design of a new generation of MB based catalysts with enhanced performance for alkane activation.

Acknowledgements

The authors wish to acknowledge the support of INVISTA Textiles (UK) Limited, INVISTA Intermediates and INVISTA Technologies S. à r. l. In addition, M.W. and C.J.K gratefully acknowledge funding from the National Science Foundation Major Research Instrumentation program (GR# MRI/DMR-1040229).

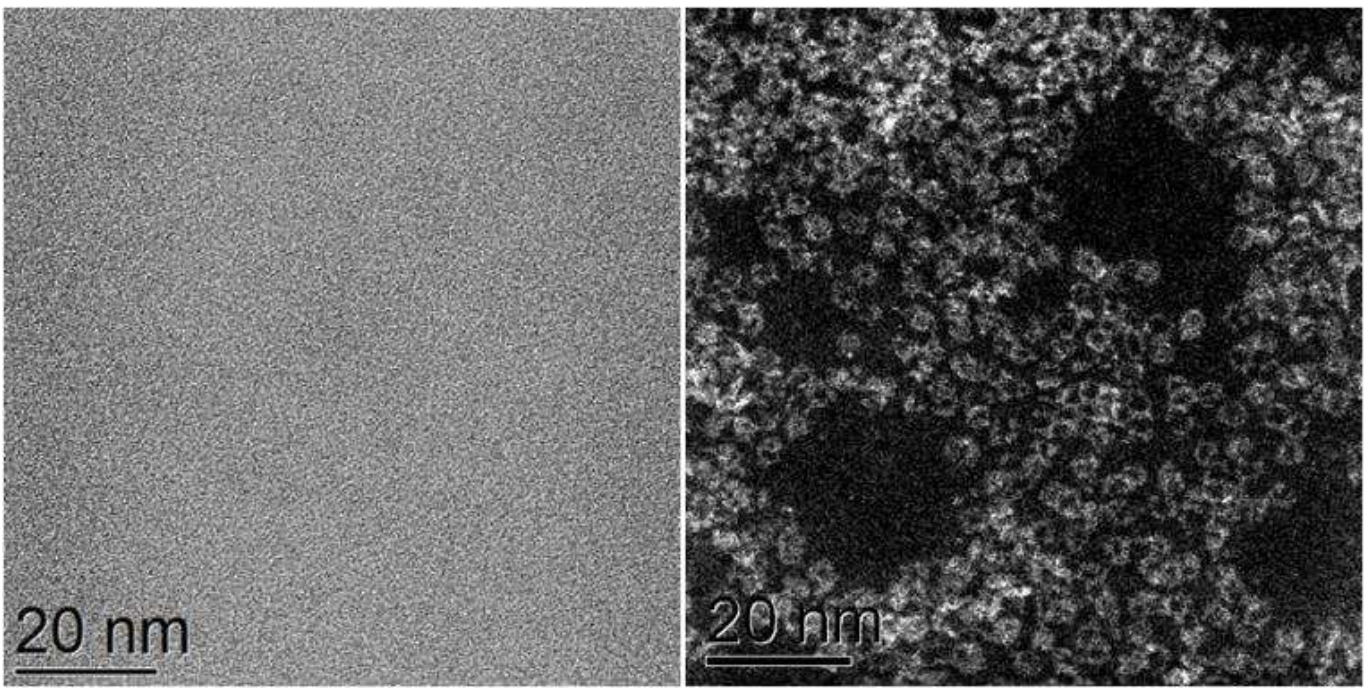

Figure 1. Comparison of the same area of an MB catalyst deposited on a continuous C film when imaged in (a) bright field (BF)-STEM mode and (b) HAADF-STEM mode.

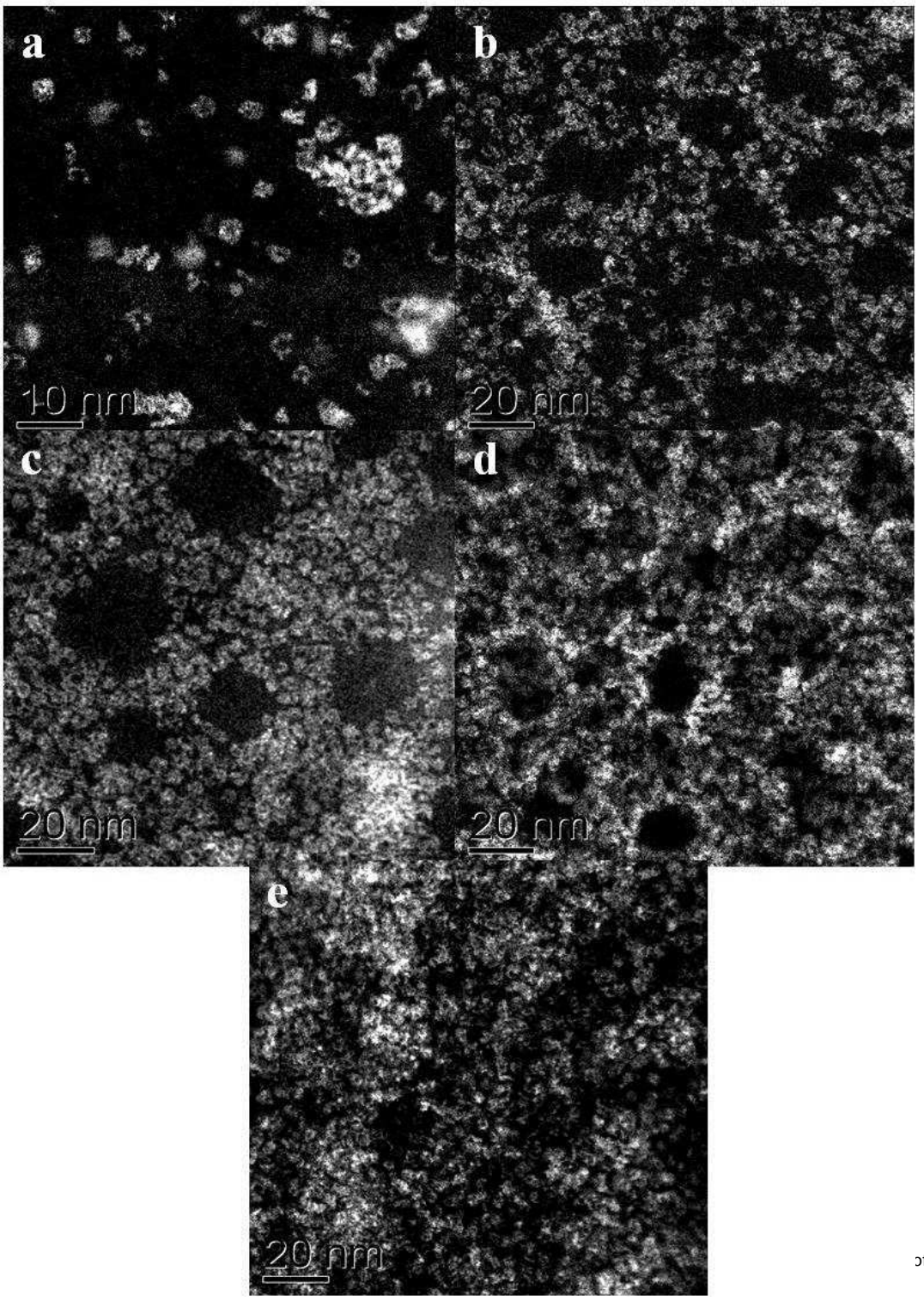
a
10 nm
b
20 nm
c
20 nm
d
20 nm
e
20 nm

Figure 2. Low-pass filtered HAADF images of samples prepared by drop casting aqueous solutions with increasing MB concentration (a)-(e) onto a holey carbon TEM grid. Low concentrations show more isolated ring structures, whereas at higher concentration the rings interact and overlap to form mesoporous self-assembled structures.

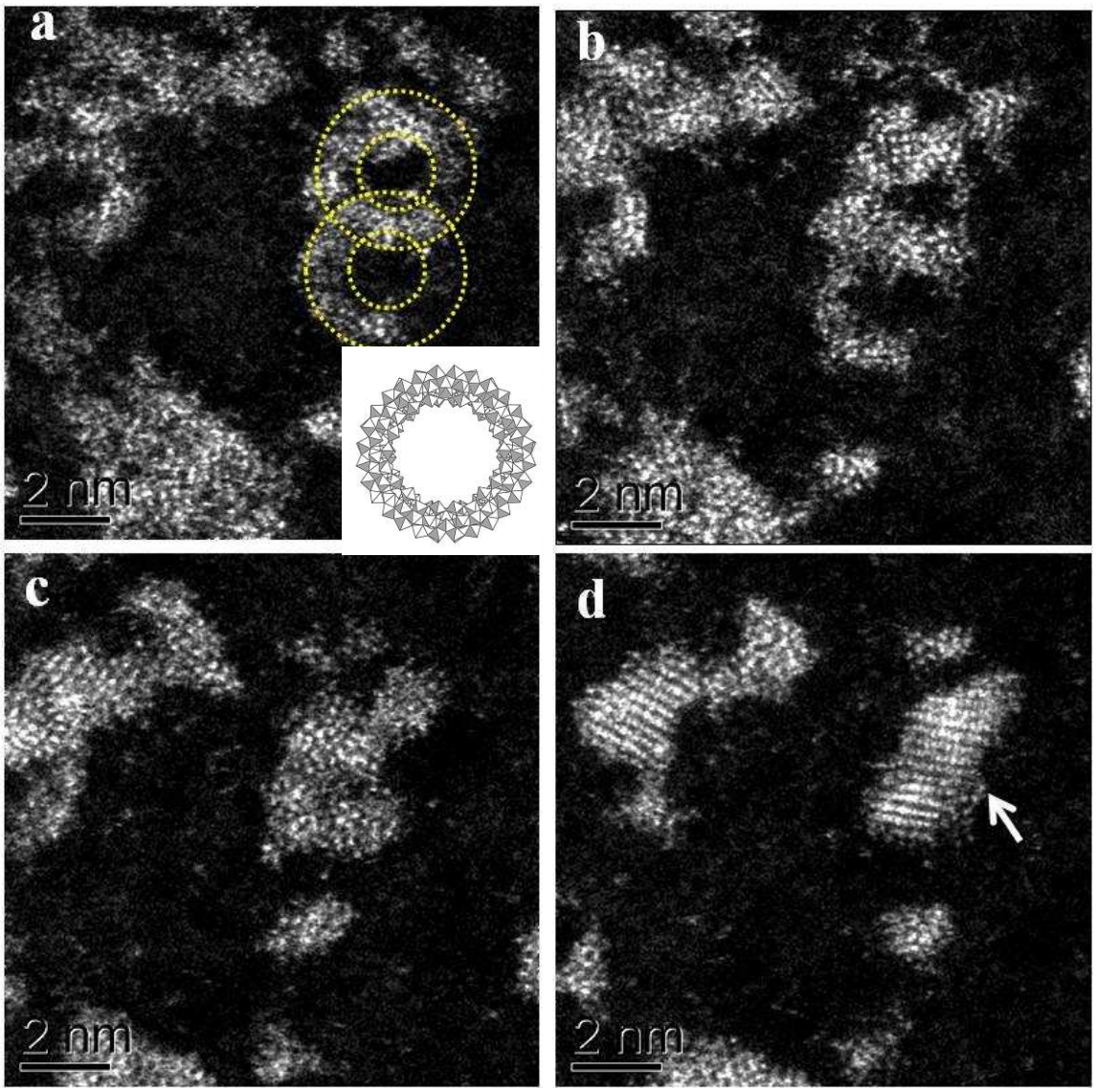

Figure 3. (a-d) A set of HAADF-STEM micrographs (low-pass filtered) of a pair of nano-rings (circled in (a)) showing the effect of electron beam irradiation on the MB material at 200kV. The images (a-c) were acquired sequentially, using a 17 s total exposure time (~ 50 pA, 200kV, 512 x 512, 64 µs/pixel) for each micrograph. Image (d) was taken under the same conditions, but after 3 minutes total exposure time. A dense crystalline phase is seen to develop from the ring structures with increasing exposure time. The crossed fringe structure in (d) can be

ascribed to the [13× 4] projection of α-MoO_3 (PDF# 04-008-4311) in which the $(1\bar{1}\,\bar{1})$ and $(71\bar{1})$ lattice planes are resolved with an intersection angle of ~83.4 °. Inset in (a) is a schematic diagram of a single $[Mo^{VI}_{126}Mo^{V}_{28}O_{462}(H_2O)_{70}]^{14-}$ ring-type molecule (after reference [5]).

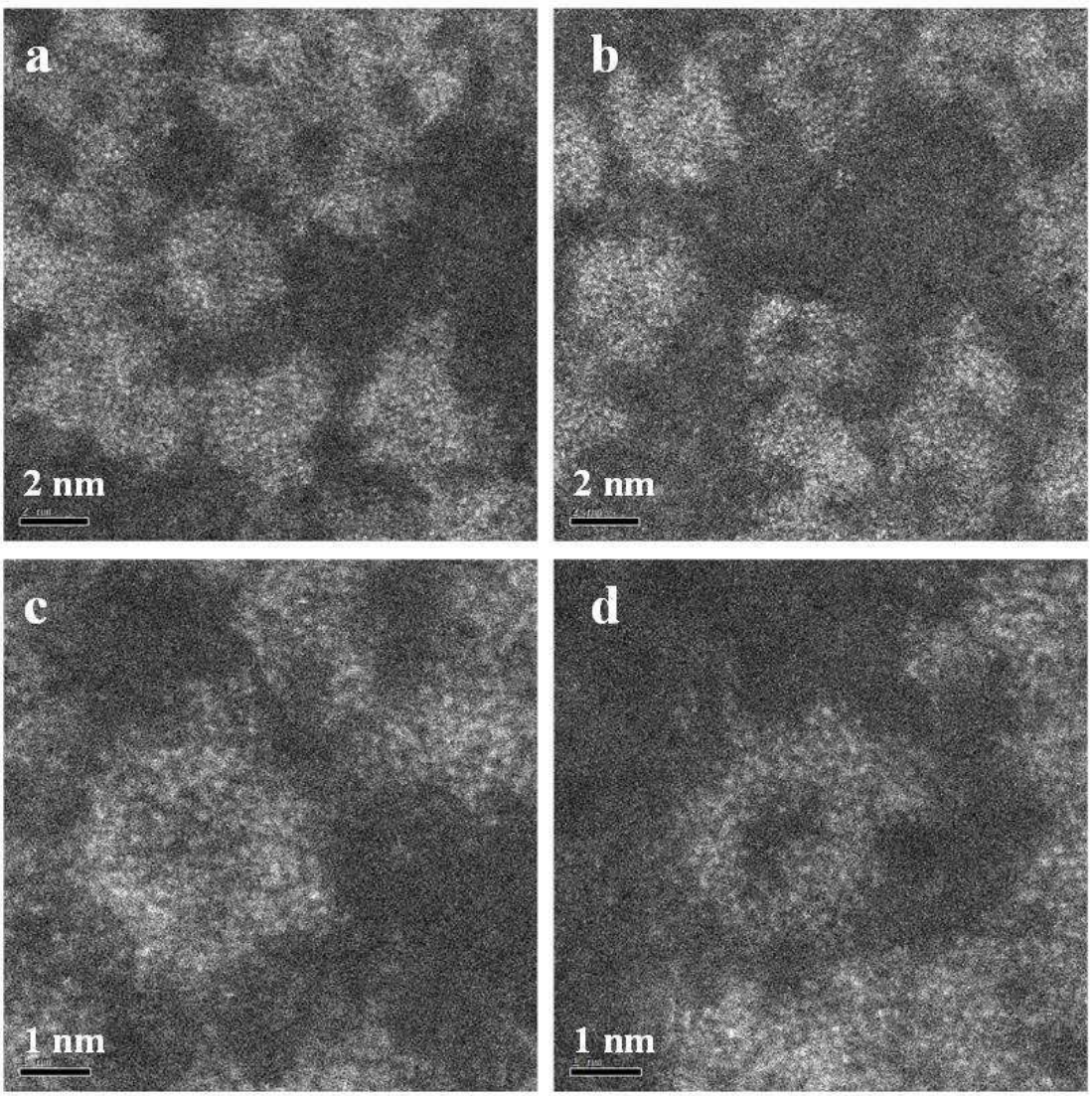

Figure 4. Representative images of MB catalysts imaged in HAADF 'gentle' STEM mode at 80kV using an aberration corrected JEOL JEM ARM 200F instrument. Mo atom positions can be discriminated within the individual rings. However, even at 80kV, there is still evidence of electron beam damage with increasing exposure time.

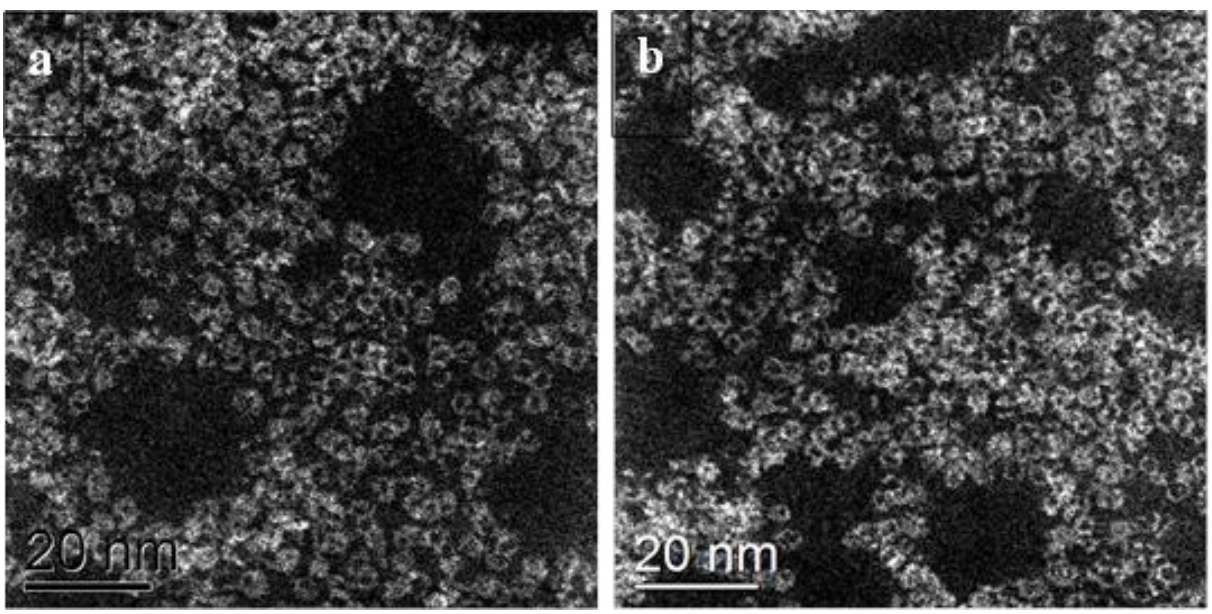

Figure 5. Low pass filtered HAADF images of the MB catalyst (a) before and (b) after reaction showing that the characteristic ring structure has been retained. Both these images were obtained at an accelerating voltage of 200kV.

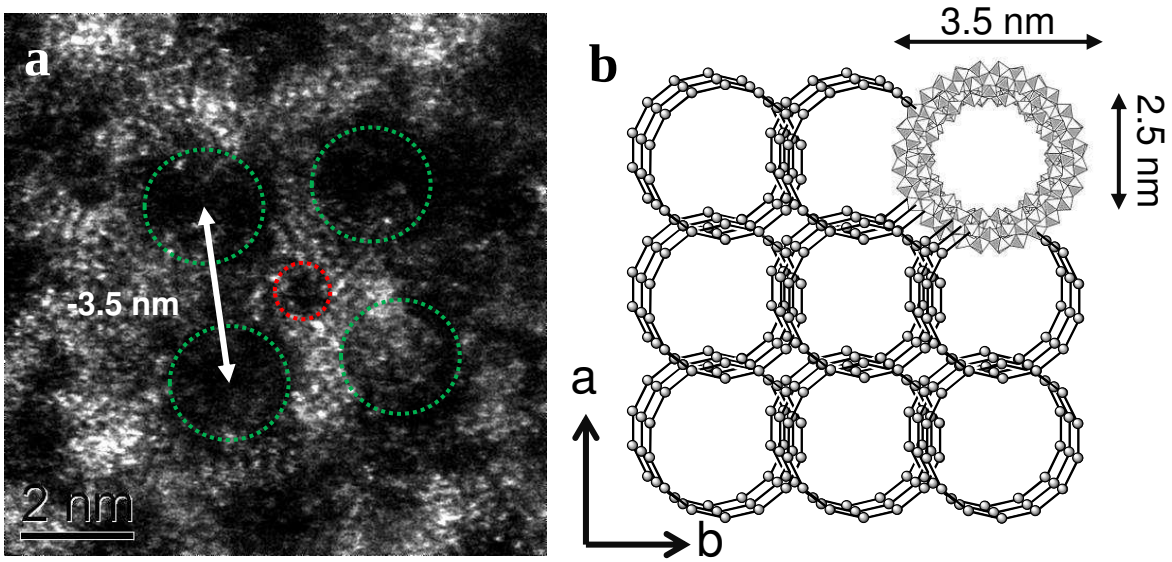

Figure 6. (a) A high magnification HAADF image of a MB sample which was prepared from a more concentrated MB solution, the Mo_{154} rings have assembled into a more ordered layered superstructure. The holespacings and separation in (a) are broadly consistent with the structure (b) of the as self-assembled superstructure determined previously by XRD (after references [5] and [7]).

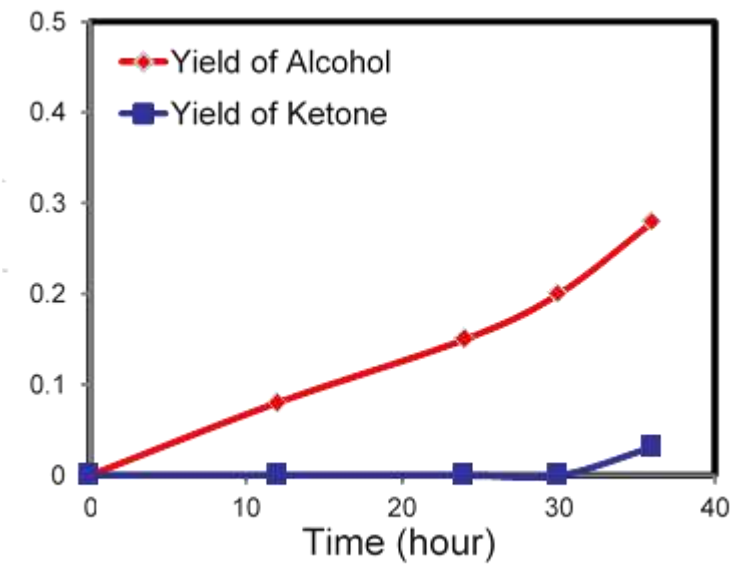

Figure 7. Catalytic performance of MB-catalysing cyclohexane oxidation as a function of reaction time (data for a hot-filtration experiment following this reaction is shown in Figure 9). Reaction conditions 8.5 g cyclohexane, 6 mg MB, 120°C, 3 bar O_2, glass reactor. Alcohol, ketone, AA and CHHP represent cyclohexanol, cyclohexanone, adipic acid andcyclohexyl hydroperoxide, respectively.

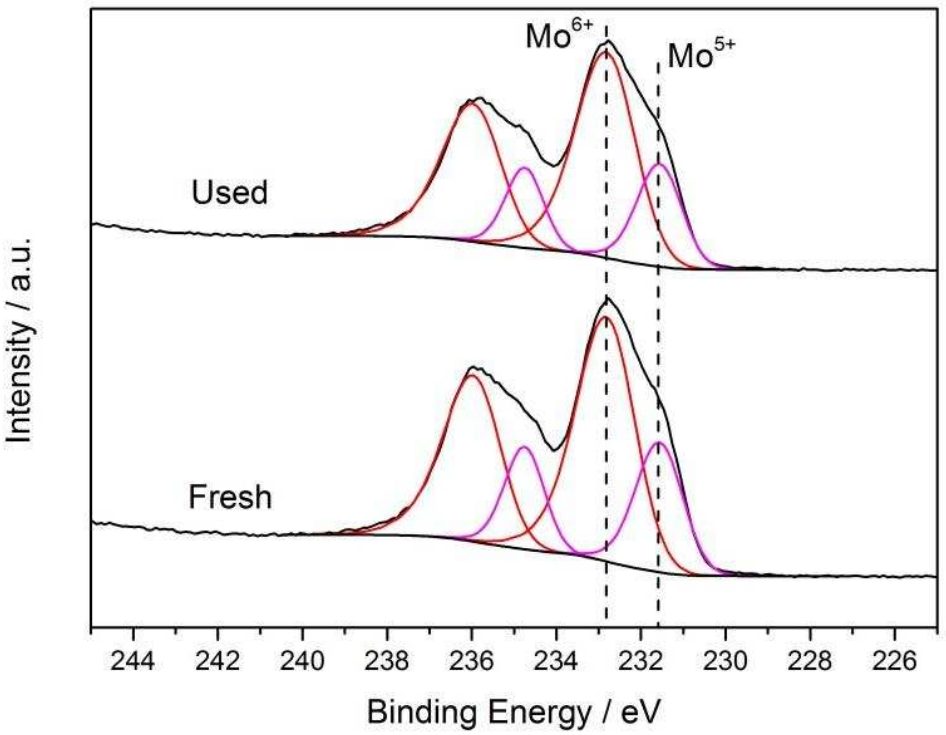

Figure 8. XPS profiles of fresh and used MB material; different Mo contributions are labelled with different colours. The relative fraction of Mo^{V} cations present in the fresh and used MB remains constant at ~20%.

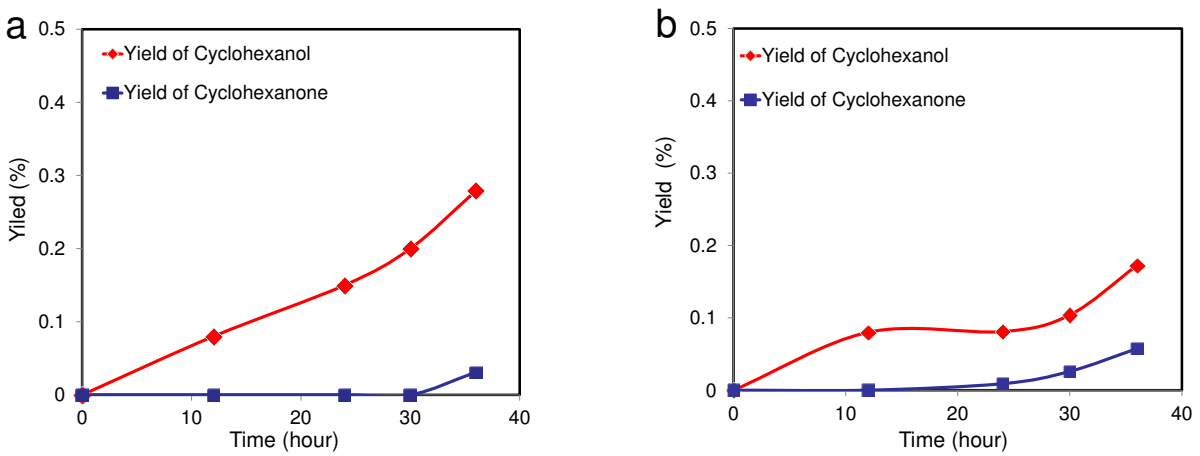

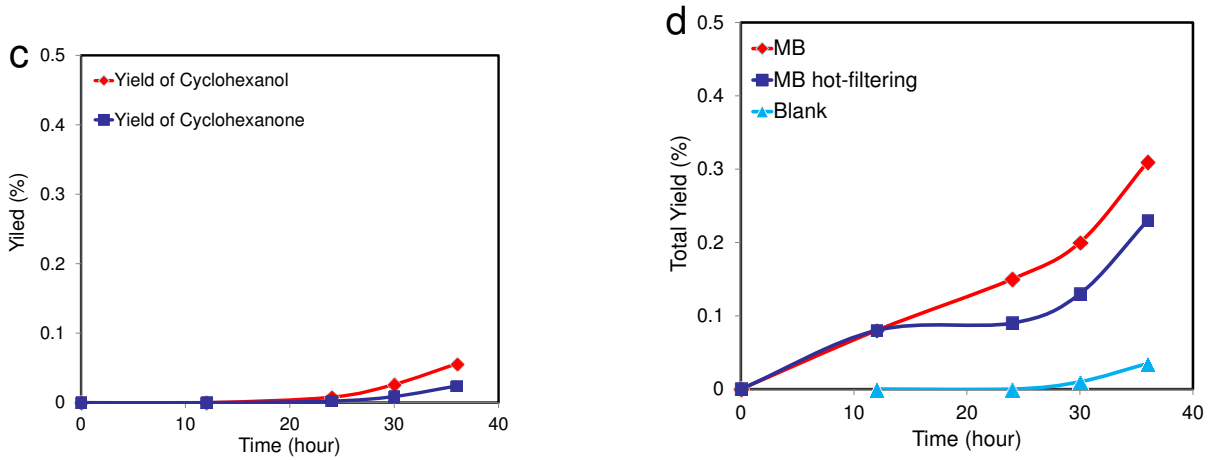

Figure 9. a) Catalytic performance of MB-catalysed cyclohexane oxidation as a function of reaction time, (reaction conditions: 10 mL cyclohexane, 6 mg MB, 120°C, 3 bar O_2, glass reactor); b) Oxidation of cyclohexane as function of reaction time after MB catalyst removal by hot filtration. In this experiment, the same reaction were employed as described above, but after 12 hours, the MB was filtered out and the filtrate was place into another clean glass reactor for continued reaction under the same reaction conditions; c) A blank experiment as a function of reaction time; d) A direct comparison of (cyclohexanol + cyclohexanone) product yield versus reaction time for the catalytic oxidation, hot filtration and blank experiments.

.

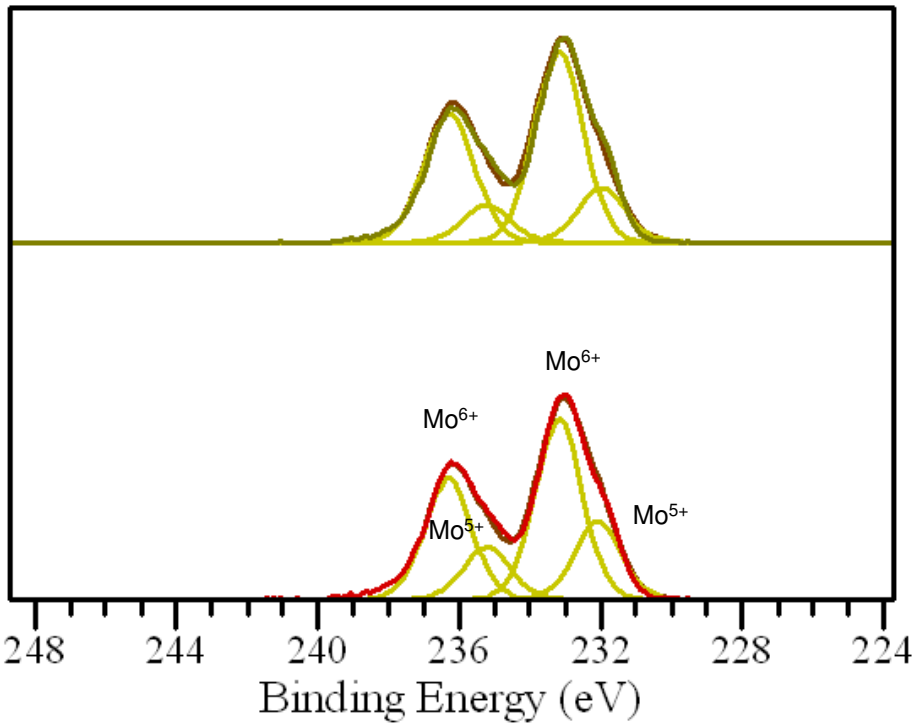

Figure 10. XPS profiles of the fresh (above) and thermally treated (below) MB samples.

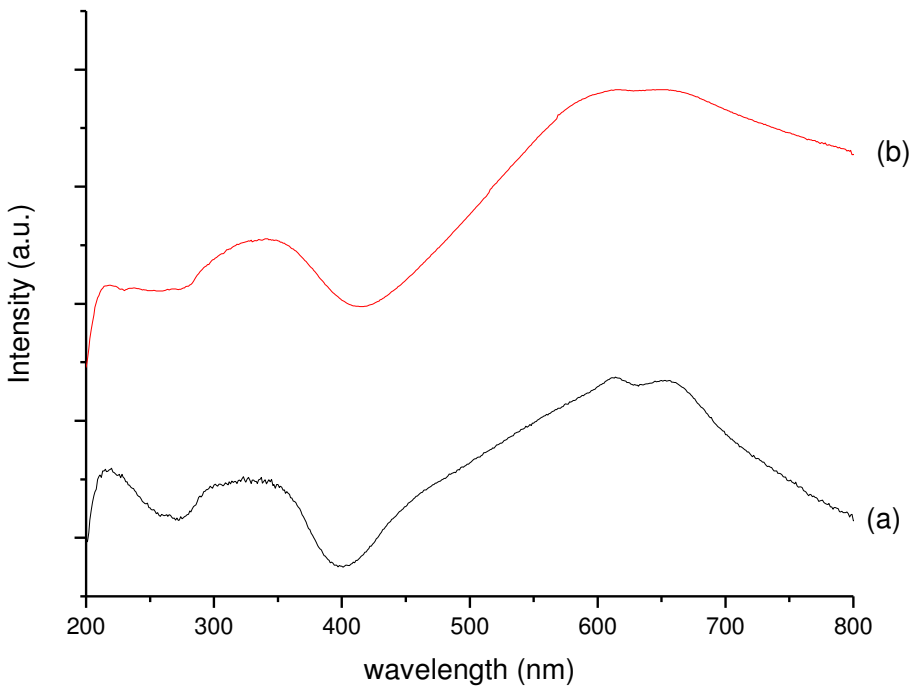

Figure 11. DR-UV/vis spectroscopy of (a) a fresh MB sample, and (b) thermally treated MB sample.

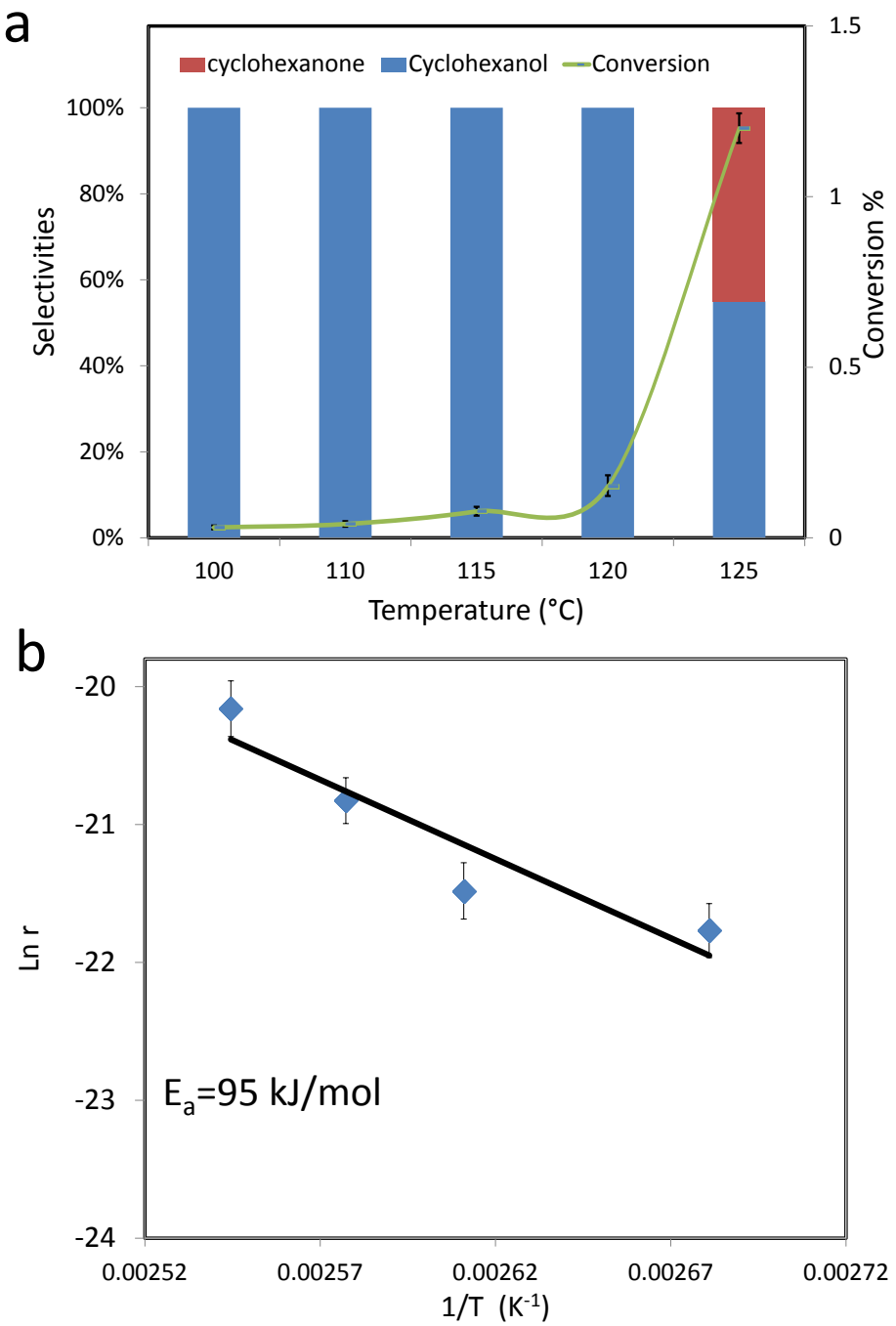

Figure 12. a) Catalytic performance of cyclohexane oxidation as a function of reaction temperature; b) Corresponding Arrhenius plot from 100°C to 120°C. Reaction conditions: 6 mg MB, 8.5 g cyclohexane, 3 bar O_2, 24 h.

Table 1. Comparison of cyclohexane oxidation using MB and a variety of other materials as catalysts.

Catalyst		Conversion (%)*	Selectivity (%)				
			A	K	CHHP	AA	Total**
1	MB	6.0	52	40	0	1	93
2	Co-naphthanate	9.0	45	37	0	2	85
3	$Fe(acac)_3$	7.7	35	48	0	0	82
4	$SiMo_{12}O_{40}$	6.0	30	50	0	9	90
5	Blank	1.1	22	19	57	0	98
6	MB***	5.5	28	49	0	20	98

*Reaction conditions, unless otherwise specified: cyclohexane (8.5 g), catalyst (6 mg), 140 °C, 3 bar O_2, 17 h reaction time. In the shorthand notation used, $Fe(acac)_3$ is Fe(III) acetylacetonate; A, K, CHHP, and AA represent cyclohexanol, cyclohexanone, cyclohexyl hydroperoxide and adipic acid respectively.

** By-products include long chain carbons and esters (see ESI†, Tables S1 and S2).

*** MB sample after thermal treatment (see section 3.2).

Table 2. Re-usability of MB in the oxidation of cyclohexane.

Number of usage cycles	Conversion (%)*	Selectivity (%)				
		A	K	CHHP	AA	Total *
1st	6.0	52	40	0	1	93
2nd	6.5	50	42	0	0	92
3rd	6.3	53	42	0	2	97
4th	6.3	52	42	0	1	95

*Reaction conditions, cyclohexane (8.5 g), catalyst (6 mg), 140 °C, 3 bar O_2, 17 h reaction time. In the shorthand notation used, A, K, CHHP and AA represent cyclohexanol, cyclohexanone, cyclohexyl hydroperoxide and adipic acid respectively.

** By-products include long chain carbons and esters.

Table 3. Catalytic performance characteristics of cyclohexane oxidation over a variety of different catalyst materials in the presence of a radical scavenger ($CBrCl_3$).

Catalyst	Conversion (%)*	Selectivity (%)					
		A	K	CHHP	BCH	AA	Total
MB	7	58	26	-	9	-	93
Co naphthenate	0.9	3	12	-	75	-	90
$Fe(acac)_3$	0.8	5	7	-	35	-	47
$SiMo_{12}O_{40}$	6.7	50	35	-	10	-	95

*Reaction conditions: 8.5 g cyclohexane, catalyst (6 mg), 140 °C, 3 bar O_2, 17 hour; $Fe(acac)_3$ represents Fe(III) acetylacetonate. In the shorthand notation used, A, K, CHHP, AA and BCH represent cyclohexanol, cyclohexanone, cyclohexyl hydroperoxide, adipic acid and bromocyclohexane respectively.

Notes and references

[a] Cardiff Catalysis Institute, School of Chemistry, Cardiff University, Cardiff, CF10 3AT, UK, hutch@cardiff.ac.uk

[b] Department of Chemistry, Dainton Building, University of Sheffield, Sheffield, S3 7HF, UK

[c] Department of Materials Science and Engineering, Lehigh University, 5 East Packer Avenue, Bethlehem, PA 18015-3195, USA

[d] INVISTA Textiles (UK) Limited, P.O. Box 2002, Wilton, Redcar, TS10 4XX, UK

†Electronic Supplementary Information (ESI) available: details of GC/MS and NMR characterization of the products and XRD and STEM of MB after thermal treatment. See DOI: 10.1039/b000000x/

1. M.G. Mellon, Analytical Absorption Spectroscopy, John Wiley and Sons Inc. 1950.
2. P. M. Huang, Y. Li, and M. E. Sumner, Handbook of Soil Sciences: Resource Management and Environmental Impacts, Second Edition, CRC Press, 2011, CH13-11.
3. M. Pansu, J. Gautheyrou, Handbook of Soil Analysis: Mineralogical, Organic and Inorganic Methods, Springer, 2007, 827.
4. C. W. Scheele, Sämmtliche physische und chemische Werke, D., Sigismund Friedrich Hermbstädt. 1793, 185-200. Digital copy available at http://reader.digitale-sammlungen.de/de/fs1/object/display/bsb10915844_00001.html
5. A. Müller, J. Meyer, E. Krickemeyer and E. Diemann, Angew. Chem. Int. Ed. 1996, **35**, 1206.
6. D. Zhong, F. L. Sousa, A. Müller, L. Chi and H. Fuchs, Angew. Chem. Int. Ed. 2011, **50**, 7018.
7. A. Müller and C. Serain, Acct. Chem. Res. 2000, **33**, 2.
8. P. Delporte, F. Meunier, C. Pham-Huu, P. Vennegues, M. J. Ledoux and J. Guille Catal. Today, 1995, **23**, 251.
9. T. Liu, E. Diemann, H. Li, A. W. Dress and A. Müller, Nature 2003, **426**, 59.
10. D. M. David Jeba Singh, T. Pradeep, J. Bhattacharjee and U. V. Waghmareb, J. Am. Soc. Mass. Spectrom. 2007, **18**, 2191.
11. B. Visic, M. Klanjsek Gunde, J. Kovac, I. Iskra, J. Jelenc and M. Remskar, Mater. Res. Bull., 2013, **48**, 802.
12. G. Li, L. Jiang, S. Pang, H. Peng and Z. Zhang, J. Phys. Chem. B. 2006, **110**, 24472.
13. Y. Kikutani, J. Mol. Catal. A: Chem., 1999, **142**, 247.
14. S. A. Schunk, Handbook of Heterogeneous Catalysis (2nd Edition), Wiley-VCH, Weimar, 2008.
15. A. M. Khenkin, L. Weiner, Y. Wang and R. Neumann, J. Am. Chem. Soc., 2001, **123**, 8531.
16. R. K. Rana and B. Viswanathan, Catal. Lett. 1998, **52**, 25.
17. R. S. da Cruz, M. M. Dauch, U. Schuchardt and R. Kumar, Stud. Surf. Sci. Catal. 2000, **130**, 1037.
18. J. A. Labinger, J. Mol. Catal. A: Chem., 2004, **220**, 27.
19. R. H. Crabtree, J. Chem. Soc. Dalton Trans., 2001, 2437.
20. U. Schuchardt, D. Cardoso, R. Sercheli, R. Pereira, R. S. da Cruz, M. C. Guerreiro, D. Mandelli, E. V. Spinace and E. L. Pires, Appl. Catal. A: General 2001, **211**, 1.
21. I. Hermans, P. A. Jacobs and J. Peeters, Chem. Eur. J., 2006, **12**, 4229.
22. B.P.C. Hereijgers, B.M. Weckhuysen, J. Catal 2010, **270**, 16
23. S.B. Turnipseed, A.J. Allentoff, J.A. Thompson, Anal. Biochem 1993, **213**, 218.
24. D. Wang, D. S. Su and R. Schlögl, Z. Anorg. Allg. Chem, 2004. **630**, 1007.
25. A. Müller, E. Krickemeyer, H. Bögge, M. Schmidtmann, C. Beugholt, S.K. Das and F. Peters, Chem. Eur. J. 1999, **5**, 1496.
26. S. Noro, R. Tsunashima, Y. Kamiya, K. Uemura, H. Kita, L. Cronin, T. Akutagawa and T. Nakamura, Angew. Chem. Int. Ed. 2009, **48**, 8703
27. J. M. Poblet, X. López and C. Bo, Chem. Soc. Rev., 2003, **32**, 297.
28. C. M. Callahan, S, C. Foti and J. R. Lai, Anal. Chem., 1960, **32**, 635.
29. M. Conte, X. Liu, D. M. Murphy, K. Whiston and G. J. Hutchings, Phys. Chem. Chem. Phys., 2012, **14**, 16279.
30. S. V. Dvinskikh, A. V. Yurkovskaya and H.-M. Vieth, J. Phys. Chem., 1996, **100**, 8125.
31. C. Berti and M. J. Perkins, J. Chem. Soc. Chem. Comm., 1979, 1167.
32. A. Dhakshinamoorthy, M. Alvaro and Hermenegildo García, ACS Catal., 2011, **1**, 48.
33. Y. Kikutani, J. Mol. Catal A: Chem., 1999, **142**, 247.
34. M. Labanowska, Phys. Chem. Chem. Phys., 1999, **1**, 5385.
35. M. Conte and V. Chechik, Chem. Commun., 2010, **46**, 3991.
36. T. Ressler, J. Wienold, R. E. Jentoft and F. Girgsdies, Eur. J. Inorg. Chem., 2003, 301.
37. A. A. Bugayev and S. E. Nikitin, Opt. Commun., 2000, **180**, 69.
38. B. P. C. Hereijgers and B. M. Weckhuysen, J. Catal., 2010, **270**, 16.
39. S. Tanase, E. Bouwman and J. Reedijk, Appl. Catal. A: Gen., 2004, 259, 101.
40. R. H. Holm, Chem. Rev., 1987, **87**, 1401.
41. J. Bäckvall, Modern Oxidation Methods, Second Edition, 2011 Wiley.
42. I. Rekkab-Hammoumraoui, A. Choukchou-Braham, L. Pirault-Roy, C. Kappenstein, Bull. Mater. Sci. 2011, **34**, 1127
43. C. Hettige, K.R.R. Mahanama andD.P. Dissanayake, Chemosphere, 2001, 43, 1079.

